

BRACS: A Dataset for BReAst Carcinoma Subtyping in H&E Histology Images

Nadia Brancati^{1*}, Anna Maria Anniciello², Pushpak Pati^{3,5}, Daniel Riccio^{1,4}, Giosuè Scognamiglio², Guillaume Jaume^{3,6}, Giuseppe De Pietro¹, Maurizio Di Bonito², Antonio Foncubierta³, Gerardo Botti², Maria Gabrani³, Florinda Feroce², and Maria Frucci¹

¹Institute for High Performance Computing and Networking of the Research Council of Italy, ICAR-CNR, Naples, Italy

²National Cancer Institute – IRCCS – Fondazione Pascale, Naples, Italy

³IBM Research – Zurich, Switzerland

⁴University of Naples Federico II, Naples, Italy

⁵ETH Zurich, Switzerland

⁶EPFL Lausanne, Switzerland

*Corresponding author: nadia.brancati@cnr.it

ABSTRACT

Breast cancer is the most commonly diagnosed cancer and registers the highest number of deaths for women with cancer. Recent advancements in diagnostic activities combined with large-scale screening policies have significantly lowered the mortality rates for breast cancer patients. However, the manual inspection of tissue slides by pathologists is cumbersome, time-consuming, and is subject to significant inter- and intra-observer variability. Recently, the advent of whole-slide scanning systems have empowered the rapid digitization of pathology slides, and enabled to develop digital workflows. These progress further enable to leverage Artificial Intelligence (AI) to assist, automate, and augment pathological diagnosis. But AI techniques, especially Deep Learning (DL), require a large amount of high-quality *annotated* data to learn from. Constructing such task-specific datasets poses several challenges, such as, data-acquisition level constrains, time-consuming and expensive annotations, and anonymization of patient information, etc. In this paper, we introduce the BReAst Carcinoma Subtyping (BRACS) dataset, a large cohort of annotated Hematoxylin & Eosin (H&E)-stained images to advance the characterization of breast lesions. BRACS contains 547 Whole-Slide Images (WSIs), and 4539 Regions of Interest (Rols) extracted from the WSIs. Each WSI, and respective Rols, are annotated by the consensus of three board-certified pathologists into different lesion categories. Specifically, BRACS includes three lesion types, *i.e.*, benign, malignant and atypical, which are further subtyped into seven categories. The included Rols exhibit large variability in dimensions, and incorporate the usual tissue-preparation and staining artifacts to bestow a realistic breast cancer diagnosis. It is, to the best of our knowledge, the largest annotated dataset for breast cancer subtyping both at WSI- and Rol-level. Further, by including the understudied atypical lesions, BRACS offers an unique opportunity for leveraging AI to better understand their characteristics. We encourage AI practitioners to develop and evaluate novel algorithms on the BRACS dataset to further breast cancer diagnosis and patient care.

Background & Summary

Histology images contain both complex and ambiguous information, thus challenging pathologists to perform a robust, reproducible and efficient analysis. Further, histology images are very large, which makes their analysis cumbersome and time-consuming. With advances in Computer-Aided-Diagnosis (CAD), AI techniques, especially Machine Learning (ML) and DL, have the potential to address the aforementioned bottlenecks¹⁻⁴. These techniques can identify discriminative morphological patterns from large datasets to diagnose histology images in a standardized and objective manner. However, there exist several challenges in adopting such techniques in digital pathology, such as, (i) the requirement of large annotated datasets, (ii) the need for sufficiently variable data to set up cross-patient experiments, (iii) the inclusion of diagnostically challenging lesions, that are generally difficult and expensive to acquire, (iv) the utilization of sub-region annotations to delineate RoI, (v) the coverage of diagnostic spectrum, and (vi) coping with data leakage and noisy annotations. Recent advancements in DL have demonstrated superior capabilities compared to classical ML approaches for CAD⁵⁻¹¹. The crucial advantage of DL approaches is their ability to learn task-specific salient features directly from the training data. However, this superiority comes at the cost of acquiring large, high-quality, variable, and unbiased annotated training datasets. Although several datasets for diagnosing breast histology images exist¹²⁻¹⁶, they do not meet all the aforementioned criteria. For instance, some datasets focus on specific diseases that include only binary classes^{12,14}, while others handling multiple classes^{13,15} include only a small number of training samples

(both at WSI- and RoI-level) collected from a few patients, thus limiting the dataset variability. Further, the set of considered classes in a dataset is crucial. Most of the public datasets aim to categorize lesions into benign and malignant classes, which do not depict the complete spectrum of classes in breast cancer diagnosis. Many of these datasets contain standardized images without clinical artifacts, *e.g.*, staining anomalies, ink marks, tissue folding, blurred regions, tears etc. Consequently, these datasets do not comprehensively represent the real-world breast cancer diagnosis. Thus, it is necessary to develop a breast cancer dataset consisting of heterogeneous images across the diagnostic spectrum which is comparable to real-world diagnosis performed by the pathologists.

To this end, we introduce BRACS, a large cohort of H&E-stained images to advance CAD of breast lesions. BRACS features the following advantages over the extant breast cancer image datasets, (i) it includes a large and heterogeneous set of realistic breast histology images (both at WSI- and RoI-level), (ii) RoIs range over variable dimensions by entirely including the diagnostic lesion, thus avoiding the loss of diagnostically relevant information, (iii) the images are acquired from a large number of patients encompassing large variability, and (iv) two atypical lesion categories, also known as precancerous lesions, are included along with other categories. In particular, we consider the following lesion types, Normal (N), Pathological Benign (PB), Usual Ductal Hyperplasia (UDH), Flat Epithelial Atypia (FEA), Atypical Ductal Hyperplasia (ADH), Ductal Carcinoma in Situ (DCIS), and Invasive Carcinoma (IC). Thus, BRACS represents a more realistic benchmark for breast cancer diagnosis by including several types of typical and atypical tissue samples over a wide variety of WSIs and RoIs extracted from a large number of patients.

Methods

The BRACS dataset is created to support the development of breast cancer diagnostic methods through the automatic analysis of histology images. The dataset was developed through the collaboration of the National Cancer Institute - Scientific Institute for Research, Hospitalization and Healthcare (IRCCS) "Fondazione G. Pascale", the Institute for High Performance Computing and Networking (ICAR) of National Research Council (CNR), and IBM Research – Zurich. The dataset was acquired from patients between 2019 and 2020, by board-certified pathologists of the Department of Pathology at the National Cancer Institute - IRCCS "Fondazione G. Pascale" in Naples (Italy). The samples were generated from H&E-stained breast tissue biopsy slides, and were selected based on the diagnostic reports of the patients. The age of the patients range from 16 to 86 years, with about 61% of patients in the range of 40-60 years, and only a few patients aging less than 20 years or above 80 years.

WSI- and RoI-level annotations

The curation of rich and comprehensively annotated histology images is a complex and time-consuming task, while being prone to observer variability. The inclusion of atypical breast lesions at both WSI- and RoI-level further increases the task complexity by requiring annotations of specialized expert pathologists. Moreover, a WSI typically includes *several* lesions of *different* subtypes. To address the aforementioned challenges, we started by extracting and annotating RoIs in WSIs, and subsequently derived the WSI-level label as the most severe cancerous lesion detected within the slide. Specifically, the RoI-level annotations were conducted in a two-step procedure. First, a set of representative RoIs in each WSI was identified. Three board-certified pathologists *independently* annotated the RoIs, *i.e.*, either as normal tissue or as one of the six lesion subtypes. Each extracted RoI corresponds to a unique category, and can include single or multiple glandular structures. Then, the annotations with disagreement were further discussed and re-annotated by the consensus of three pathologists. This process ensures reliable annotations, and allows to alleviate inter- and intra-observer variability. Figure 1 presents the annotation procedure for a sample WSI and its corresponding RoIs. All the RoIs were extracted and annotated with the help of QuPath¹⁷. The number of extracted RoIs per WSI ranges from 0 to 119, with an average of 11 RoIs per WSI. Multiple RoIs corresponding to different lesion subtypes were selected per WSI such that the collected RoIs across all WSIs collectively encompass the lesion heterogeneity. This aspect is very crucial for representing pathogenesis and disease progression, and consequently allowing for the inclusion of sufficiently variable data for DL model training. Subsequently, the WSI-level labels were trivially defined as the most aggressive tumor subtype annotated in the image.

Subtype annotations

An important characteristics of BRACS is the inclusion of atypical lesions, ADH and FEA. While ignored in other public datasets, these categories remain important as they might be indicators of either (i) the presence of abnormalities in neighboring breast tissue that could go undetected, *e.g.*, due to the extraction of small tissue samples, or (ii) a high risk of onset of future carcinoma, *i.e.*, development of DCIS and IC. In addition, these lesions cannot be detected by mammography or other breast imaging techniques, nor can they be felt during a clinical breast examination. When detected in a core biopsy, more frequent imaging follow-up and often surgical excision are recommended¹⁸. BRACS also includes lesion subtypes belonging to benign and malignant types. In particular, benign lesions are subtyped as either non-cancerous lesions (PB) or inflammatory responses

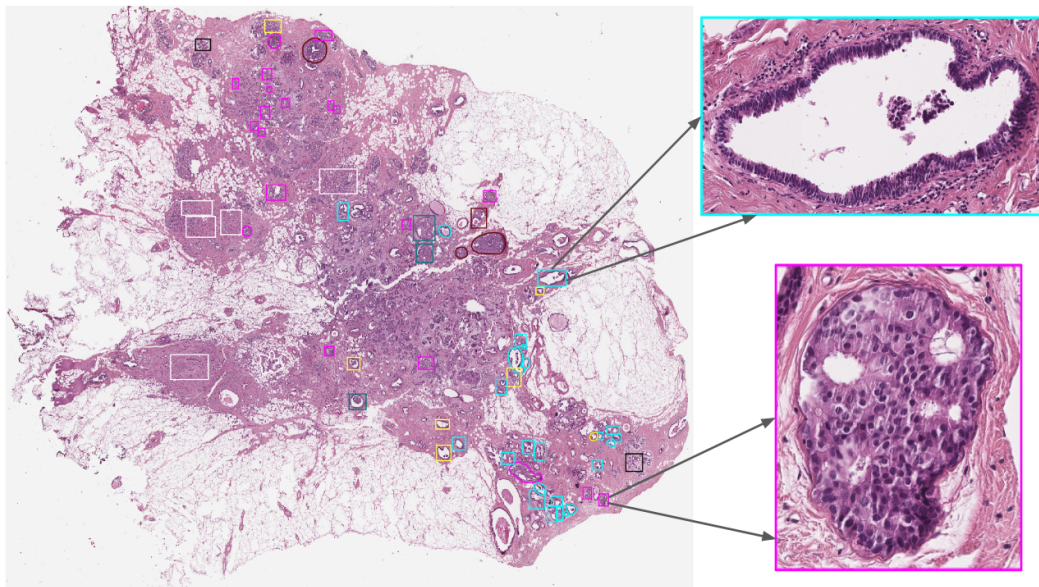


Figure 1. Example of a WSI and its associated RoIs. The color of each contour indicates the tumor subtype of the lesion according to a fixed color palette.

(UDH). Malignant lesions are categorized as either DCIS or IC. Finally, histology images representing normal tissue sample are classified in the Normal (N) category.

In order to clarify the description of the different tissue subtypes, a brief description of the mammary gland should be considered. The breast is a modified apocrine sweat gland, made up of 15-25 independent glandular units called lobes, each of which is formed by a compound tubulo-acinar gland. The lobes are comprised of adipose tissue and divided by connective tissue septa. Inside each lobe, the main ducts branch into terminal ducts, each of which leads to a lobule that is made up of many berries to form the ductulo-lobular terminal unit. Detailed information on lesions included in BRACS can be found in¹⁹. The specific features of the different sample tissue subtypes are shortly summarized in the following and a representative example for each of them is shown in Figure 2.

Normal Tissue (N)

In normal mammary glandular tissue, there are two types of epithelial cells (the luminal layer and the basal myoepithelial layer) and two types of stromal cells (interlobular stroma and intralobular stroma). Differently from PB, the ratio between epithelial component and stroma is preserved.

Pathological Benign (PB)

Benign breast lesions can be grouped according to the risk of developing invasive carcinoma and include several groups of histological entities classified in relation to morphology. In our study, for reasons of differential diagnosis, in the PB category we included both non-proliferative lesions and proliferative lesions with the exception of UDH, FEA and ADH, which were considered as three independent subtypes. Therefore, PB includes cyst, apocrine metaplasia, ductal ectasia, squamous metaplasia, atrophy, stromal fibrosis, mastitis, sclerosing adenosis, papilloma, radial scar, simple and complex fibroadenoma.

Usual Ductal Hyperplasia (UDH)

UDH is characterized by an increase in the epithelial layers. It is a cohesive proliferation of disorderly distributed but oriented cells. It can have different architectural aspects (solid pattern, fenestrated pattern, micropapillary pattern). Even if UDH shares some architectural features with ADH and DCIS, it does not show atypia.

Flat Epithelial Atypia (FEA)

FEA is a proliferative lesion characterized by low grade cytological atypia, cell monomorphism, loss of polarity and orientation with respect to the basement membrane, presence of apical snout, endoluminal secretion and frequent calcifications.

Atypical Ductal Hyperplasia (ADH)

ADH is a proliferation of monomorphic cells, which only partially fill the ductal spaces. Architectural aspects include a solid pattern, a cribriform pattern and a papillary pattern. The cytologic atypia is similar to that of low-grade DCIS, but the lesion

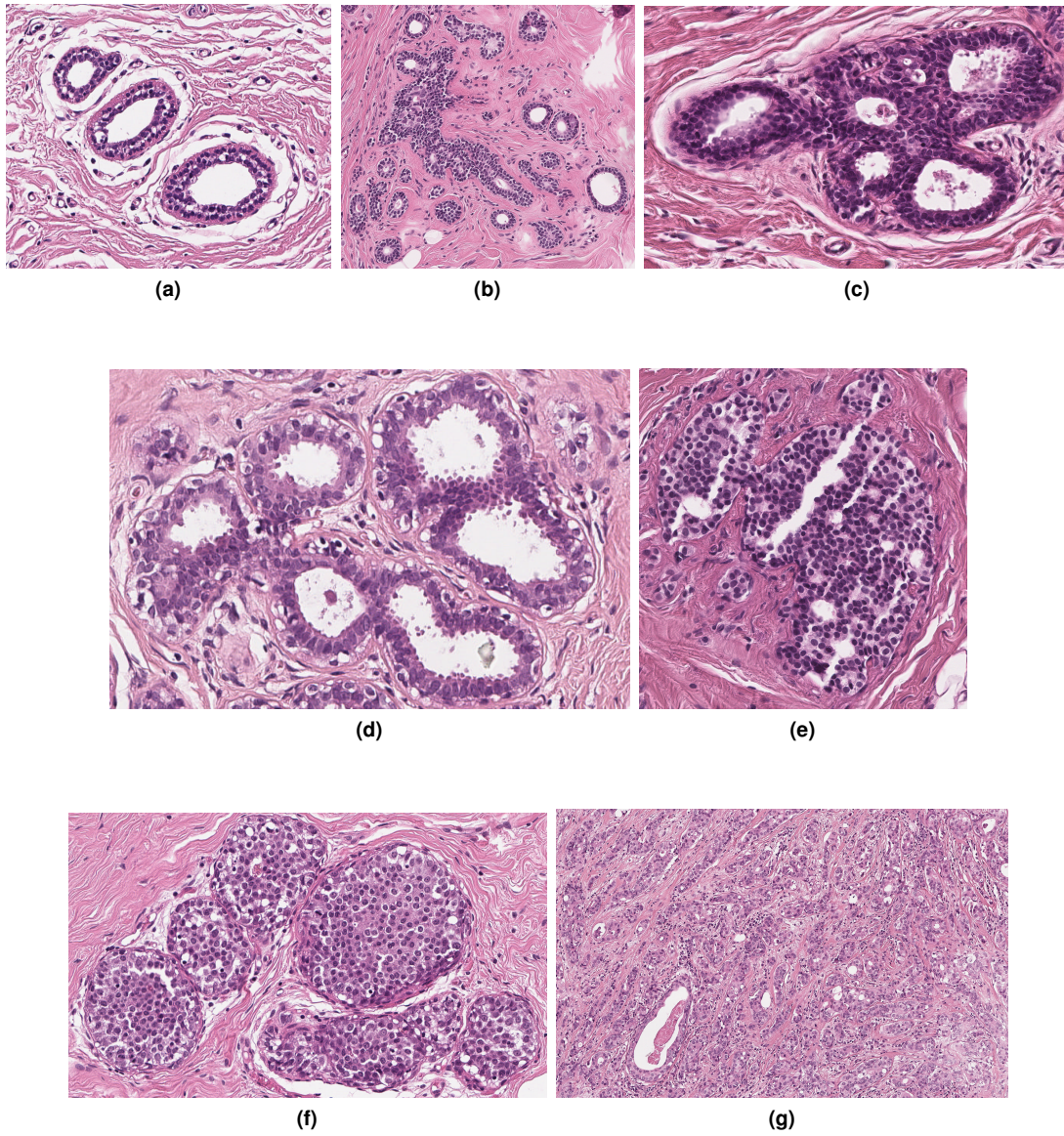


Figure 2. Examples of different tissue samples: (a) Normal (N), (b) Pathological Benign (PB), (c) Usual Ductal Hyperplasia (UDH), (d) Flat Epithelial Atypia (FEA), (e) Atypical Ductal Hyperplasia (ADH), (f) Carcinoma in Situ (DCIS) and (g) Invasive Carcinoma (IC).

spans no more than 2mm or has an insufficient architectural atypia involving only partially ducts and / or lobules.

Ductal Carcinoma in Situ (DCIS)

In situ carcinoma is a malignant proliferation of epithelial cells that fills the entire duct, without evidence of stroma invasion. Typically it involves multiple adjacent ductal spaces. It can have cribriform, solid, papillary and micropapillary patterns.

Invasive Carcinoma (IC)

IC is characterized by the invasion of tumor cells infiltrating the breast stroma with loss of peripheral myoepithelial cells. The presence of the myoepithelial cell layer is an important distinction of DCIS from IC.

Detecting certain subtypes is particularly challenging as some morphological patterns can be shared by several classes. For instance, ADH shares morphological similarities with DCIS. In certain cases, it even includes all the features of DCIS, but is simply limited in size. Also, UDH, ADH and DCIS are all characterized by an intraductal growth pattern, which makes these classes difficult to classify and differentiate in H&E-stained sections. This is particularly true when pathologists cannot utilize significant WSI-level context. We emphasize that when classifying BRACS RoIs, no context information is provided beside the tissue lesion and immediate tissue micro-environment.

BRACS dataset characteristics

The BRACS dataset contains 547 WSIs extracted on 189 different patients. It also includes 4'539 RoIs extracted from 387 WSI collected on 151 patients. All slides were scanned with an Aperio AT2 scanner at $0.25 \mu m/pixel$ using a magnification factor of $40\times$. Table 1 and Table 2 report the number of WSIs (with and without RoIs) and RoIs according to the lesion type and subtypes, respectively.

| Data | Benign | Atypical | Malignant | Total |
|-------------------|---------------|-----------------|------------------|--------------|
| WSIs with RoIs | 149 | 75 | 163 | 387 |
| WSIs without RoIs | 116 | 14 | 30 | 160 |
| WSIs | 265 | 89 | 193 | 547 |
| RoIs | 1837 | 1263 | 1439 | 4539 |

Table 1. BRACS data distribution according to lesion type.

| Data | N | PB | UDH | FEA | ADH | DCIS | IC |
|-------------------|----------|-----------|------------|------------|------------|-------------|-----------|
| WSIs with RoIs | 17 | 77 | 55 | 34 | 41 | 51 | 112 |
| WSIs without RoIs | 27 | 70 | 19 | 7 | 7 | 10 | 20 |
| WSIs | 44 | 147 | 74 | 41 | 48 | 61 | 132 |
| RoIs | 484 | 836 | 517 | 756 | 507 | 790 | 649 |

Table 2. BRACS data distribution according to lesion subtype.

Comparison with existing datasets

In recent years, several data sets have been proposed, with more and more samples and classes^{20–25}. Table 3 details existing public datasets of histology images for breast lesion classification. Datasets that are (i) either no more accessible²¹, (ii) subsets of already mentioned datasets²², or (iii) targeting specific tasks, *e.g.*, lesion proliferation scores prediction²⁴, pN-stage prediction²⁵, are not mentioned in Table 3.

The IDC¹² and Camelyon16²³ datasets are focusing on the detection of the presence of a given lesion. In particular, IDC provides RoIs at small spatial resolution (50×50 pixels) extracted from large areas of Invasive Ductal Carcinoma. We emphasize that even if the number of RoIs in BRACS is lower than in IDC, BRACS images are on average much larger allowing the inclusion of whole glandular areas. BRACS includes a larger number of WSIs than Camelyon16 and more subtypes. BreakHis²⁶ and BACH²⁰ datasets are devoted to multi-classification tasks, but remain significantly smaller than BRACS, both in terms of image size and number of samples, and include less subtypes than BRACS.

In conclusion, the number of WSIs, RoIs and associated patients, is significantly larger in BRACS compared to the existing public datasets. Moreover, BreakHis and BACH include fixed-size RoIs, while BRACS images are of arbitrary size. Assuming fixed-size tumor regions is a strong assumption that does not apply in real-life scenarios. Limiting the size of RoIs imposes to either (i) partially cut the lesion, hence producing a loss of information that could be pivotal for a correct diagnosis, or (ii) manually curating RoIs such that they all have similar sizes, which does not encompass tumor heterogeneity. By proposing

| Dataset, Year | Lesion Classes | | Data Type Size (Magnification) | n. Pat. | Resolution in pixels |
|--|---|---|---|---------|-------------------------|
| | Benign | Malignant | | | |
| Invasive Ductal Carcinoma (IDC) ¹² , 2014 | IDC negative | IDC positive | <i>RoI</i> 277.524 (40x) | 162 | 50x50 |
| BreakHis ¹³ , 2015 | Adenois Fibroadenoma Phyllodes tumor Tubular adenona | Carcinoma Lobular carcinoma Mucinous carcinoma Papillary carcinoma | <i>RoI</i> 1.995 (40x) 2.081 (100x) 2.013 (200x) 1.820 (400x) | 82 | 700x460 |
| Camelyon16 ²³ , 2016 | Normal Benign | In-situ carcinoma invasive carcinoma | <i>WSI</i> 400 (20x and 40x) | 400 | Variable Size |
| BACH ²⁰ , 2018 | Normal Benign | In-situ carcinoma invasive carcinoma | <i>RoI</i> 400 (200x) | 39 | 2048x1536 |
| | | | <i>WSI</i> 10(20x) | 10 | Variable Size |

Table 3. Popular publicly available breast histopathology image dataset.

| Dataset, Year | Lesion Classes | | | Data Type Size (Magnification) | n. Pat. | Resolution in pixels |
|----------------------------|-------------------------|------------|---|-----------------------------------|---------|-------------------------|
| | Benign | Atypical | Malignant | | | |
| BRACS ²⁷ , 2021 | Normal Benign UDH | FEA ADH | In-situ carcinoma invasive carcinoma | <i>RoI</i> 4537 (40x) | 151 | Variable size |
| | | | | <i>WSI</i> 547 (40x) | 189 | Variable size |

Table 4. General information on BRACS dataset

samples of varying sizes, BRACS promotes the development of DL algorithms that need to be able to operate on inputs of different dimensionality. BRACS is also the first dataset to include pre-cancerous atypical lesions. BRACS and BACH share the same malignant lesion subtypes, while BreakHis refines this class by partitioning it into four specific subtypes. All the benign lesion subtypes defined in BACH and BreakHis are also included in BRACS (normal and benign). In addition, BRACS includes UDH lesion subtype that is not considered in BACH and BreakHis.

In summary, BRACS characteristics are unique, as it allows for multi-class classification task of breast cancer lesions, including challenging atypical lesions. BRACS is also larger than the existing datasets in terms of number RoIs, WSIs and patients.

Dataset splitting

To foster reproducibility and following ML best practices, we provide pre-defined WSI- and RoI-level splits in training, validation and test sets. Data split was generated such that all the WSIs extracted from a patient belong to the *same* set. Similarly, all the RoIs extracted in a given WSI are assigned to the *same* split. By following this approach, we avoid that different sets include correlated patient- and slide-level information, that could be leading to overly optimistic prediction results²⁸. Table 5 and Table 6 present the number of WSIs included in the train, validation, and test splits. Information about the number of patients in each set is provided in Table 5. Equivalent information for RoIs is shown in Table 7 and Table 8. At RoI-level, the ratio between the most common subtype (PB with 714 samples) and the least common one (N with 357) is around two. At WSI-level, the most common subtype is PB with 120 samples and the least common one is FEA with 24 samples, hence of ratio of around four. Considering the constraint of patient- and WSI-level split, and the fact that atypical lesions are more rare than malignant ones, BRACS offers a rather balanced set, that can directly be used for training DL systems.

| | Benign | Atypical | Malignant | Total WSIs | Total Patients |
|------------|--------|----------|-----------|------------|----------------|
| Train | 203 | 52 | 140 | 395 | 133 |
| Validation | 30 | 14 | 21 | 67 | 25 |
| Test | 32 | 23 | 32 | 85 | 31 |

Table 5. WSI-level split according to the lesion type.

| | N | PB | UDH | FEA | ADH | DCIS | IC |
|------------|----------|-----------|------------|------------|------------|-------------|-----------|
| Train | 27 | 120 | 56 | 24 | 28 | 40 | 100 |
| Validation | 10 | 11 | 9 | 6 | 8 | 9 | 12 |
| Test | 7 | 16 | 9 | 11 | 12 | 12 | 20 |

Table 6. WSI-level split according to the lesion subtype.

| | Benign | Atypical | Malignant | Total WSIs | Total Patients |
|------------|---------------|-----------------|------------------|-------------------|-----------------------|
| Train | 1460 | 1011 | 1186 | 3657 | 106 |
| Validation | 135 | 90 | 87 | 312 | 15 |
| Test | 242 | 162 | 166 | 570 | 30 |

Table 7. RoI-level split according to the lesion type.

| | N | PB | UDH | FEA | ADH | DCIS | IC |
|------------|----------|-----------|------------|------------|------------|-------------|-----------|
| Train | 357 | 714 | 389 | 624 | 387 | 665 | 521 |
| Validation | 46 | 43 | 46 | 49 | 41 | 40 | 47 |
| Test | 81 | 79 | 82 | 83 | 79 | 85 | 81 |

Table 8. RoI-level split according to the lesion subtype.

Data organization

The BRACS dataset can be publicly accessed and downloaded via the BRACS website²⁷. Anyone registering and agreeing with the terms of use (Creative Commons CC0 license) can freely download it. Once registered, the user can access the FTP server containing all the data.

The data are organized as follows. The WSIs are stored in the *Whole Slide Image Set* folder, that includes the train, validation, and test data. Each data split folder is further partitioned in Benign (BY), Atypical (AT) and Malignant (MT) folders, each of which includes folders corresponding to lesion subtypes. The WSIs are stored as .svs files. All the files follow the same naming convention. For instance, the file *BRACS_1238.svs* refers to the slide ID 1238, whose label is defined by the name of the folder that contains it. The RoIs are stored in the *Region of Interest Set* folder, which follows the same structure as the WSI set. The files are stored in .png format, where the file *BRACS_1238_PB_32.png* refers to the RoI number 32, extracted from the WSI named *BRACS_1238.svs*, and labeled as Pathological Benign. The folder also includes a *previous_versions* archive that contains a .zip file with data that have been used in a series of publications during the dataset collection process, e.g.,^{29–32}. The WSI annotations are stored in the *The Whole Slide Image Annotations* folder, which follows the same structure as the WSI set. It includes annotation files in .qpdata format (based on QuPath¹⁷) for visualizing the RoIs inside their corresponding WSI. Finally, a summary file is provided as an .xlsx file, which reports for each WSI, its label, reference set (training/validation/test), corresponding patient ID and the number of associated RoIs, if any. Figure 3 highlights the folder organization of BRACS.

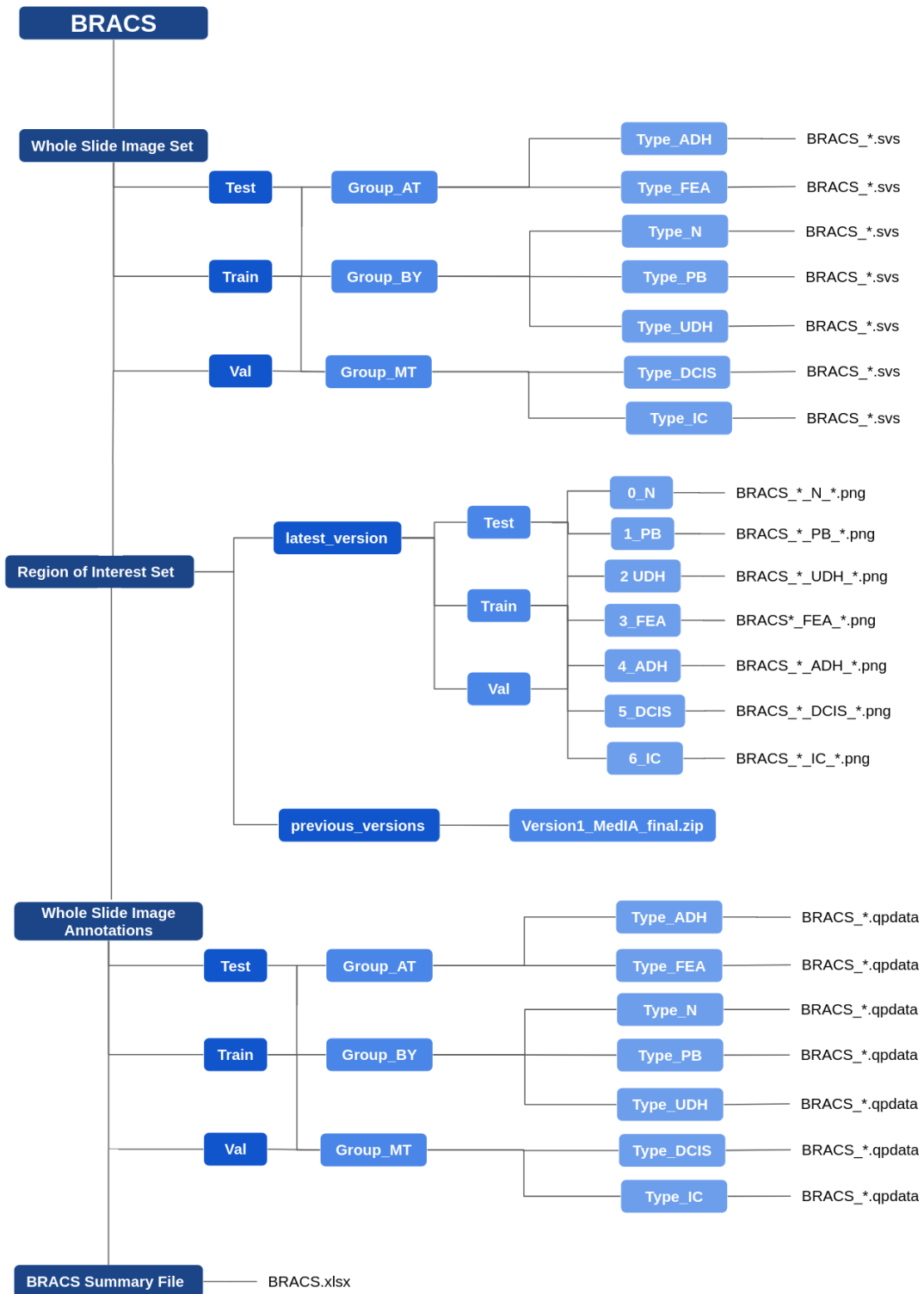


Figure 3. The organization of BRACS dataset folders.

References

1. Madabhushi, A. & Lee, G. Image analysis and machine learning in digital pathology: Challenges and opportunities. *Med. image analysis* **33**, 170–175 (2016).
2. Tizhoosh, H. R. & Pantanowitz, L. Artificial intelligence and digital pathology: challenges and opportunities. *J. pathology informatics* **9** (2018).
3. Srinidhi, C. L., Ciga, O. & Martel, A. L. Deep neural network models for computational histopathology: A survey. *Med. Image Analysis* 101813 (2020).
4. de Matos, J., Ataky, S. T. M., de Souza Britto, A., Soares de Oliveira, L. E. & Lameiras Koerich, A. Machine learning methods for histopathological image analysis: A review. *Electronics* **10**, 562 (2021).
5. Araújo, T. *et al.* Classification of breast cancer histology images using convolutional neural networks. *PloS one* **12**, e0177544 (2017).
6. Bardou, D., Zhang, K. & Ahmad, S. M. Classification of breast cancer based on histology images using convolutional neural networks. *Ieee Access* **6**, 24680–24693 (2018).
7. Sudharshan, P. *et al.* Multiple instance learning for histopathological breast cancer image classification. *Expert. Syst. with Appl.* **117**, 103–111 (2019).
8. Duggento, A., Conti, A., Mauriello, A., Guerrisi, M. & Toschi, N. Deep computational pathology in breast cancer. In *Seminars in cancer biology* (Elsevier, 2020).
9. Benhammou, Y., Achchab, B., Herrera, F. & Tabik, S. Breakhis based breast cancer automatic diagnosis using deep learning: Taxonomy, survey and insights. *Neurocomputing* **375**, 9–24 (2020).
10. Sharma, S. & Mehra, R. Conventional machine learning and deep learning approach for multi-classification of breast cancer histopathology images—a comparative insight. *J. digital imaging* **33**, 632–654 (2020).
11. Chugh, G., Kumar, S. & Singh, N. Survey on machine learning and deep learning applications in breast cancer diagnosis. *Cogn. Comput.* 1–20 (2021).
12. Idc: Invasive ductal carcinoma. <http://www.andrewjanowczyk.com/use-case-6-invasive-ductal-carcinoma-idc-segmentation/> (2014).
13. Spanhol, F. A., Oliveira, L. S., Petitjean, C. & Heutte, L. A dataset for breast cancer histopathological image classification. *IEEE Transactions on Biomed. Eng.* **63**, 1455–1462 (2015).
14. Bejnordi, B. E. *et al.* Diagnostic assessment of deep learning algorithms for detection of lymph node metastases in women with breast cancer. *Jama* **318**, 2199–2210 (2017).
15. Aresta, G. *et al.* Bach: Grand challenge on breast cancer histology images. *Med. image analysis* **56**, 122–139 (2019).
16. Veta, M. *et al.* Predicting breast tumor proliferation from whole-slide images: the tupac16 challenge. *Med. Image Analysis* **54**, 111–121 (2019).
17. Bankhead, P. *et al.* Qupath: Open source software for digital pathology image analysis. *Sci. reports* **7**, 1–7 (2017).
18. Ingegnoli, A. *et al.* Flat epithelial atypia and atypical ductal hyperplasia: carcinoma underestimation rate. *The breast journal* **16**, 55–59 (2010).
19. Breast tumors. WHO classification of tumours series, 5th ed., vol.2. *WHO Classif. Tumors Editor. Board. Lyon (France): Int. Agency for Res. on Cancer 2019* (2010).
20. Bach: The grand challenge on breast cancer histology images. <https://iciar2018-challenge.grand-challenge.org/Dataset/> (2018).
21. Roux, L. *et al.* Mitosis detection in breast cancer histological images an icpr 2012 contest. *J. pathology informatics* **4** (2013).
22. Bioimaging 2015 breast histology classification challenge. <http://www.bioimaging2015.ineb.up.pt/dataset.html> (2015).
23. Camelyon 2016: Camelyon grand challenge 2016. <https://camelyon16.grand-challenge.org/Data/> (2016).
24. Tupac16: Tumor proliferation assessment challenge 2017. <http://tupac.tue-image.nl/> (2016).
25. Camelyon 2017: Camelyon grand challenge 2017. <https://camelyon17.grand-challenge.org/> (2017).
26. Breakhis: Breast cancer histopathological database breakhis. <http://web.inf.ufpr.br/vri/databases/breast-cancerhistopathological-database-breakhis/> (2015).

27. BRACS: BReAst Carcinoma Subtyping. <https://bracs.icar.cnr.it> (2021).
28. Bussola, N., Marcolini, A., Maggio, V., Jurman, G. & Furlanello, C. Ai slipping on tiles: Data leakage in digital pathology (2021).
29. Pati, P. *et al.* Hact-net: A hierarchical cell-to-tissue graph neural network for histopathological image classification. In *Medical Image Computing and Computer Assisted Intervention (MICCAI) Workshop on GRaphs in biomedicAl Image anaLysis* (2020).
30. Pati, P. *et al.* Hierarchical graph representations in digital pathology. In *Medical Image Analysis* (2021).
31. Jaume, G. *et al.* Towards explainable graph representations in digital pathology. In *International Conference on Machine Learning (ICML), Workshop on Computational Biology* (2020).
32. Jaume, G. *et al.* Quantifying explainers of graph neural networks in computational pathology. In *IEEE Conference on Computer Vision and Pattern Recognition (CVPR)* (2021).

Acknowledgements

We would like to acknowledge Engr. Alessandro Manzoni from the IRCCS Fondazione Pascale for his support for management of technical instruments. We would like to acknowledge Ph.D Mario Sicuranza from ICAR-CNR for the development and technical implementation of the BRACS site.

Author contributions statement

National Cancer Institute- IRCCS-Fondazione Pascale, Naples, Italy
Anna Maria Anniciello, Gerardo Botti, Maurizio Di Bonito, Florinda Feroce, Giosuè Scognamiglio

Institute for High Performance Computing and Networking-CNR, Naples, Italy
Nadia Brancati, Giuseppe De Pietro, Maria Frucci, Daniel Riccio

IBM Zurich Research Lab, Zurich, Switzerland
Pushpak Pati, Guillaume Jaume, Antonio Foncubierta, Maria Gabrani

Contributions

All authors have provided critical feedback during revision process and actively participated in preparation of the manuscript. G.B., G.D.P and M.G. were responsible for the conceptualization of this project. A.F and M.F. contributed to the conceptualization and were responsible for execution and management of this project. M.D.B. was responsible for the institutional clinical databases and contributed to the annotation process. A.M.A. and F.F. contributed to the clinical design of the dataset, data annotations and documentation for the project and organization of the validation of results. P.P., N.B. and G.J. contributed to the dataset organization and validation. G.S. collected cases, extracted and scanned slides from their institutional clinical databases. D.R. contributed to the conceptualization of this project.